# Wireless, Accumulation Mode Dosimeters for Monitoring Pulsed and Non-Pulsed Germicidal Lamps

Seung Yun Heo, Kyeongha Kwon, Michelle Chan, Philipp Gutruf, Alex Burton, Tony Banks, Chongwen Duan, Hokyung Jang, Jeonghyun Kim, Daniel Franklin, Jun Bin Park, and John A. Rogers, *Fellow, IEEE*

Abstract—Mitigating the spread of infectious diseases such as the one associated with the COVID-19 pandemic demands simple and effective disinfection techniques. Ultraviolet germicidal irradiation (UVGI) is one such method, in common use for decontamination of hospital rooms. Practical technologies designed to monitor UVGI ensure the delivery of sufficient doses for germicidal efficacy. Existing UVGI dosimeters rely on intermittent measurements of intensity as the basis for a numerical integration scheme that approximates dose. Traditional devices are ineffective, particularly with pulsed UVGI lamps that emit pulses of light with durations shorter than the interval of measurement. Here, we present a compact, accumulation mode dosimeter (AMD) that detects continuously, as opposed to intermittently, at single or multiple UVGI wavelengths. The AMD utilizes an array of photodiodes and supercapacitors to passively transduce and capture photocurrent generated by UVGI without the use of external power. The accumulated voltage across the supercapacitors then serves as a measure of UVGI dose. A key result is that sampling intervals of AMD do not constrain measurement accuracy. When implemented with a wireless transponder, AMD supports a light-adaptive sampling scheme designed to adjust the sampling interval to the intensity and period of UVGI exposure. Compared to time-based sampling schemes adopted by conventional sensors, light-adaptive approaches autonomously optimize battery life by minimizing current consumption during periods of low or no UVGI. Benchtop studies of the use of this technology with pulsed Xenon lamps (pulse ~5 ms) sampled at long intervals (>1s) highlight the key features of operation. Demonstration of AMD during UVGI of *E.* Coli cultures represents an example in dose dependent effects on disinfection.

Index Terms—Low-power electronics, wireless communication, dosimetry, ultraviolet sources, radiation monitoring, electronics circuits.
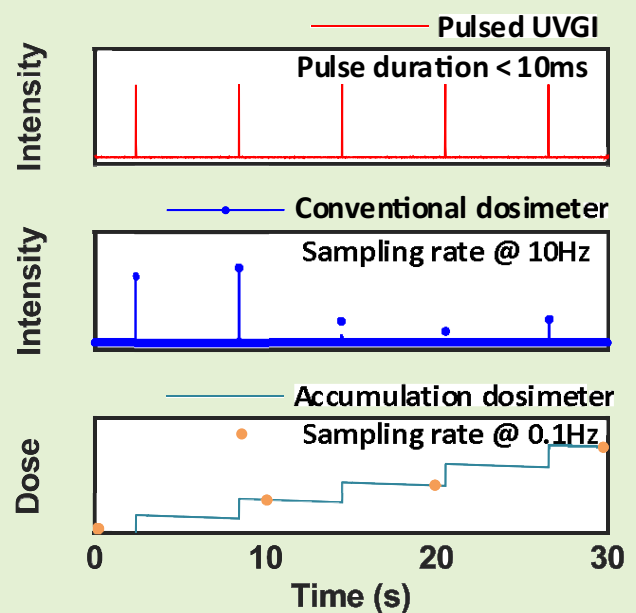
I. INTRODUCTION

THE coronavirus pandemic and similar disease outbreaks that are likely to occur in the future demand effective and efficient protocols for decontamination. Disinfection of personal protective equipment (PPE) and hospital rooms reduces pathogen burden and prevents nosocomial transmissions. Ultraviolet germicidal irradiation (UVGI) is one of the most promising techniques, as recommended by the Centers for Disease Control (CDC) for disinfection of filtering facemasks and hospital equipment [1]–[4]. Exposure to UV light effectively inactivates pathogens by denaturizing nucleic acid bases that form RNAs. Delivery of an appropriate UV dose renders damage to RNA, thereby blocking viral replication [5], [6]. The threshold dose for disinfection depends on the type of irradiant UV, namely UVA (315 – 400 nm), UVB (280 – 315 nm), or UVC (200 – 280 nm). The spectral absorbance of nucleotides peaks at 260 nm and decreases with increasing wavelength [7]. Correspondingly, UVC is the most lethal wavelength, while UVB and UVA are less efficient in damaging RNA [8], [9].

Dosimeter technologies that monitor exposures to germicidal irradiation can ensure safe protocols for reliable disinfection. Wavelength and dose directly affect germicidal

TABLE I
SUMMARY OF EXISTING UVGI DOSIMETERS

Company	Data Acquisition	Dimensions (mm)	Interface	Max Sampling per 1s	Power Source	Cost ($)
ExTech	Time-Stamping	182x73x47	LCD/ SD memory	1	6 AA	1190
General Tools	Time-Stamping	140x49x29	LCD	1	9V	650
Omega	Time-stamping	177x68x45	LCD/ USB cable	1	6 AA	850
Sper Scientific	Time-Stamping	140x49x30	LCD	1	9V	670
Larson Electronics	Time-Stamping	159x77x42	LCD	2.5	9V	960
Analytik Jena	Time-Stamping	157x51x91	LCD	2.8	9V	930
Solarmeter	Button-Operation	106x61x22	LCD	3	9V	250
Linshang Tech	Time-Stamping	148x76x26	LCD	6	4 AAA	450
International Light Technologies	Time-Stamping	152x76x40	LCD/ USB cable	50	USB charging	2440
Gigahertz-Optik	Time-Stamping	145x63x30	LCD/ USB cable	4k	2 AA	2400

efficacy [10], and underexposure significantly diminishes effectiveness [11], [12]. At the same time, overexposure can accelerate degradation of polymers [13] and other common materials in practical settings. For example, high dose exposures can compromise the structural integrity of PPE such as filtering face respirators [14], [15]. Traditional approaches to digital dosimetry during UVGI rely on intensity-sampling strategies that detect the power of irradiance at programmed time intervals, with approximate interpolative integration schemes to determine dose. This approach leads to measurement errors when the sampling rate is slower than the frequency of pulsed light sources [16]. An accurate measurement is particularly challenging during scenarios of exposure to short-pulsed, high-intensity germicidal lamps commonly used in hospitals and industrial settings [17]–[20]. A list of existing digital sensors for wireless dosimetry of UVGI is in Table I. In most systems, sampling rates of portable platforms are <10 readings per second. Wireless dosimeters or wired data acquisition hardware with fast sampling rates are costly, on a scale of several thousand dollars, and are impractical for pulsed UVGI applications.

A recently reported dosimetry scheme, first introduced in miniaturized, wireless dosimeters designed for measurements of exposure to sunlight, overcomes this drawback. This approach exploits a continuous mode of operation based on an accumulation mode dosimeter (AMD) module, [21], [22]. Here, a photodiode and a supercapacitor electrically connected in parallel transduce and store the effects of cumulative light exposure in the form of accumulated voltage across the supercapacitor, as a measurement that can be calibrated to the total exposure energy per area. A key feature is that this approach measures accumulated dose directly, independent of

sampling rate and without power consumption. This paper introduces a single- and multi-wavelength detection platform for UVGI based on a wireless embodiment of the AMD approach, including capabilities in UVC measurements via appropriate wavelength-selective photodiodes.

Results demonstrate accurate dosimetry during exposure to germicidal light sources, including high power Xenon lamps that generate millisecond pulses. An example in *E. Coli* disinfection illustrates the use of single-wavelength UVC dosimeters of this type, as well as multi-channel versions that also operate in the UVA and UVB regions.

II. MATERIALS & METHODS

A. System Architecture

1) Single-Channel, UVC Dosimeter: The single-wavelength, UVC dosimeter (Fig 1A) is a small (13 mm × 16 mm × 4 mm), wireless platform designed to continuously detect cumulative dose of exposure to UVC, as shown in Fig 1B&C. The top side includes a collection of UVC photodiodes (PDs) and supercapacitors (SCs; Fig 1D). The bottom supports a Bluetooth system-on-chip (BLE SoC) with peripheral components, a mechanical switch, and a MOSFET (Fig 1F). A coin cell battery (diameter 14mm, capacity 27mAh) rests between top and bottom layers (Fig 1E).

The circuit diagram is in Fig 1G. In the presence of UVC radiation, the UVC PDs generate photocurrent (I_{ph}) that charges a collection of SCs connected in parallel. The accumulated voltage across the SCs (V_{sc}) depends linearly on the UVC dose [21]. The number of PDs and the capacitance of the SCs define the detection sensitivity and range of operation of the AMD module. Activation of a MOSFET triggers wireless discharge of the SCs if V_{sc} exceeds a selected
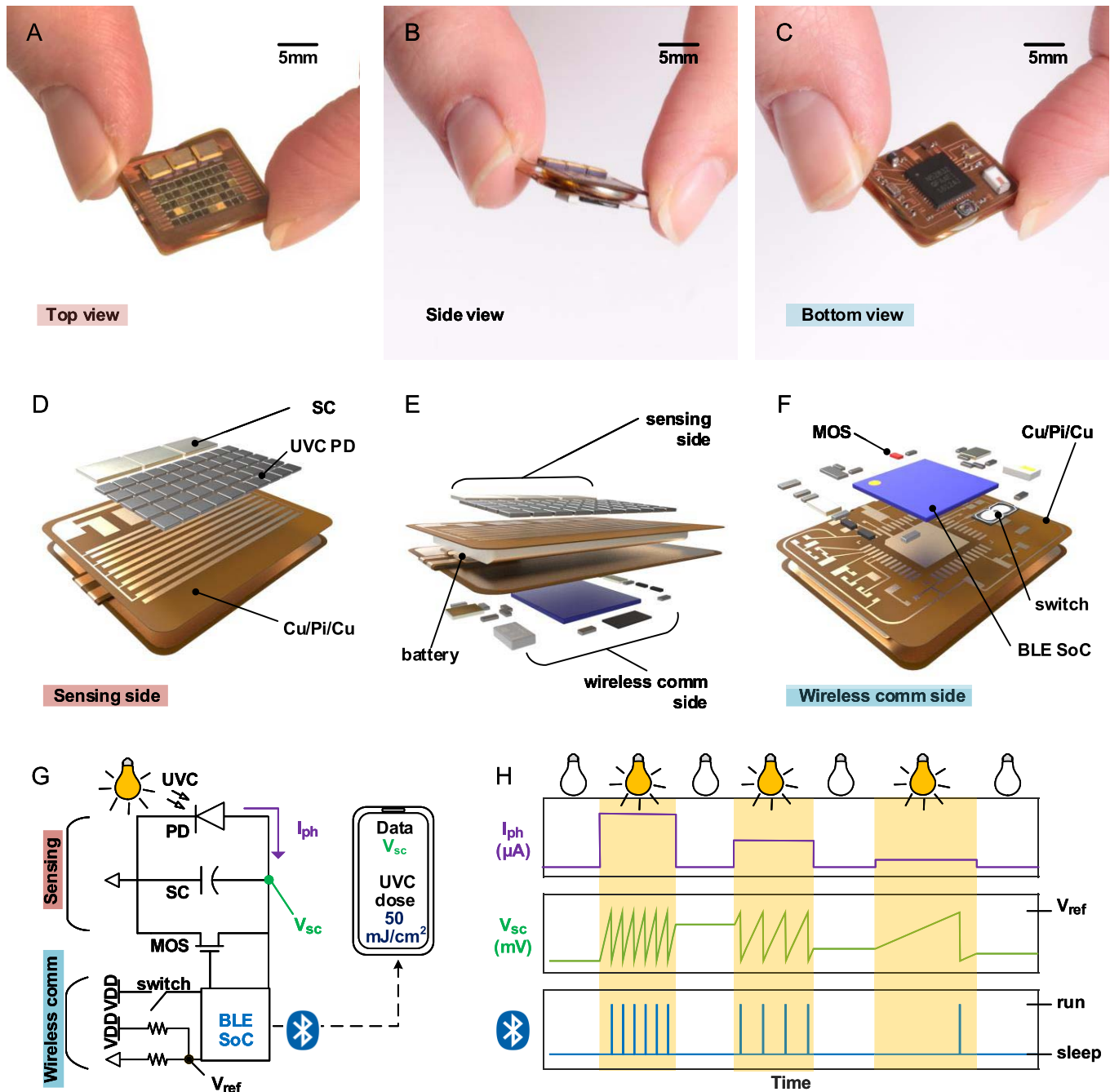
Fig. 1.   **System Architecture** (A,B,C) Photographs of an accumulation-mode dosimeter for monitoring germicidal light. (D, E, F). Exploded view diagrams of layers and components. The top side of the device supports an array of UVC photodiodes (PD) and supercapacitors (SC). A copper/polyimide/copper laminate serves as the substrate. The bottom side consists of a Bluetooth System-on-Chip (BLE SoC), a MOSFET (MOS), a mechanical switch, and auxiliary components. A battery rests in between the top and bottom layers. (G) Circuit diagram and wireless pairing with a smartphone. In the presence of UVC, the PD generates photocurrent (I_{ph}) and the SC accumulates voltage proportionally. The voltage across the supercapacitor (V_{sc}) is a measurement of UVC dose. If $V_{sc} < V_{ref}$, the BLE SoC remains in 'deep-sleep', the lowest power mode of operation. V_{ref} is the threshold voltage to 'wake' BLE SoC. If $V_{sc} > V_{ref}$, the BLE SoC enters 'run-mode.' The 'run' sequence is read and send V_{sc} to a paired smartphone, discharge V_{sc} via activation of MOS, read and send V_{sc} after discharge, then return to 'deep-sleep' if $V_{sc} < V_{ref}$. The switch enables a 'force-wake' function. (H) Schematic illustration of light-adaptive communication. The PD generates I_{ph} proportional to UVC power which charges V_{sc}. The BLE SoC remains in 'deep-sleep' in absence of UVC. The BLE SoC enters 'run' mode and sends wireless alerts to a paired smartphone when $V_{sc} > V_{ref}$.

threshold voltage (V_{ref}). The BLE SoC is responsible for wireless data transfer and MOSFET switching.

Traditional IMDs utilize UVC PDs to generate I_{ph}, which is amplified and applied to an analog to digital converter (ADC) as a measurement of intensity. The circuit diagram of typical

IMDs is in SFig1a. IMDs require a transimpedance amplifier to convert I_{ph} to a voltage readable by ADC. Then, the ADC chip drives an output on a liquid crystal display (LCD) at a selected sampling interval. A battery powers the transimpedance amplifier, the ADC, as well as the LCD. On the other

hand, the AMD presented here detects UVC dose without external power and requires a battery solely to power the BLE SoC. AMDs use supercapacitors to passively convert I_{ph} to voltage during continuous UVGI detection. Functional diagrams of the AMD and IMD architectures are in SFig1. For both systems, increasing the sampling rate increases the average current consumption and decreases the battery life [16], [23].

2) Light-Adaptive Sampling Scheme: To optimize battery-life, AMD leverages the lack of dependence on sampling rate by automatically adapting sampling interval according to light conditions, [22] as described schematically in Fig 1H. In detail, when the UVC light source is 'off', the BLE SoC remains in a low-power 'deep-sleep' mode, where power supply passes only to a real-time clock and a sub-block that contains a Low-Power Comparator (LPCOMP) to compare V_{sc} to V_{ref}. When the UVC source is 'on', V_{sc} increases with time of exposure, as a measure of dose. If V_{sc} exceeds V_{ref}, then the BLE SoC 'wakes up' and enters 'run mode,' as mapped in SFig2. The current consumed by BLE SoC in 'run mode' ($\sim 10\ \mu A$) is >20 fold compared to current consumed in 'deep-sleep' ($\sim 0.4\ \mu A$). In 'run' mode, the BLE SoC 1) digitizes V_{sc} and wirelessly transfers this information to a separate BLE-enabled device (e.g. tablet, smartphone, etc), 2) activates the MOSFET to discharge the supercapacitors, and then 3) returns to 'deep-sleep' mode. As a result, the frequency of BLE communication depends on both the intensity and duration of exposure to UVC, as the cumulative exposure dose. For on-demand data transfer, the device also incorporates a mechanical switch to force the BLE SoC into 'run mode'.

3) Multi-Channel, UVGI Dosimeter: The basic device architecture of Fig. 1 can be extended easily for operation at multiple wavelengths across the UV range. A multi-wavelength dosimeter designed to separately operate in the UVA, UVB, and UVC regions utilizes three ADC channels of the BLE SoC and three separate AMD modules. Specifically, arrays of UVA, UVB, or UVC PDs in parallel to three separate arrays of SCs and three MOSFETs establish three detection channels. In this study, the detection spectra for the UVA, UVB, and UVC PDs are 320 – 400 nm, 240 – 320 nm, and 220 – 280 nm, respectively, with maxima at 350 nm, 300 nm and 254 nm, respectively. A connection between the UVC channel and the LPCOMP of the BLE SoC establishes UVC as the trigger for 'wake up'. When V_{sc} accumulated by the UVC PDs exceeds V_{ref}, the BLE SoC 'wakes up', wirelessly transmits data for all three channels, discharges all SCs, and returns to 'deep-sleep.' Any wavelength can be selected as the trigger channel. For UVGI, UVC is the primary wavelength of interest because it is known to be the most effective germicidal wavelength.

B. Fabrication

The fabrication and assembly processes use off-the-shelf components and flexible printed circuit board technology. A UV laser system (LPKF U4, LPKF Inc) ablated circuit traces on a flexible substrate (Pyralux AP8535R, DuPont Inc) of bonded copper/polyimide/copper layers (thickness $111\mu m$). An electroplating system (LPKF Contac S4, LPKF Inc) electrically bridged vias from the top to the bottom copper layers. Heated solder paste established robust connections between the interconnects on flexible printed circuit board and the off-the-shelf surface-mount-devices (SMD). SMDs included photodiodes (GUVC-S10GD, GenUV; GUVC-S40GD, GenUV; COB2418PKG, GenUV; SM1206, Bivar), supercapacitors (CPX3225A, Seiko), and Bluetooth System-on-Chip (nRF52832, Nordic Semiconductor). A 3V coin cell battery (CR1216, Murata) powered the BLE SoC. The total bill of materials was $\sim$\$230.

C. Preparation, Treatment, and Analysis of E. Coli

This study includes a demonstration of UVGI on *Escherichia* coli (E. Coli) with simultaneous dosimetry. E. Coli (Strain: DH5α) samples were obtained from Thermo Fisher. The E coli ($100\mu l$, 1×10^7 in LB medium) concentrated onto sterile filter paper discs (10 mm in diameter). Blanket discs served as negative controls and unirradiated discs served as positive controls. A low-pressure mercury-arc lamp (UVP EL 254 nm, Analytik Jena) placed 35 cm above irradiated the samples (n = 3) continuously for various times. A button operated UVC meter (UVC8.0, Solarmeter) measured the UVC intensity before and after each treatment. The AMD device measured the exposure dose during each treatment. Irradiated and non-irradiated samples were separately cultured in Lysogeny broth and incubated at 37°C for 22 hours. To quantify bacterial density, a spectrophotometer (Cytation5, Biotek) measured OD600. Measurements of OD600 compared to negative and positive controls determined the absence or presence of bacteria, respectively, in samples treated with varying UVGI doses.

III. EXPERIMENTS & RESULTS

A. UVC Dosimetry of a Pulsed Xenon Lamp

IMD modules measure the total incident power on the PDs at pre-programmed time intervals and then numerically integrate over time by interpolation between successive measurements to yield estimates of cumulative exposure dose. For scenarios that involve time dependent exposure levels, the timing of these measurements, specifically the sampling rate, can limit the accuracy. The use of Xenon lamps (Fig 2A) that emit germicidal light in a pulsed mode with durations $\sim$ 5 ms at intervals of 6 s represent such a scenario. UVC emission from such a lamp measured by a commercial UVC meter with a maximum sampling rate of 3 Hz is in SFig 3a. Over a representative time of 200 s, the meter captures less than 60% of the pulses. To accurately profile pulsed irradiation with $\sim$ 5 ms pulses, the sampling rate should be greater than 200 Hz. A wired high bandwidth data acquisition system connected to a UVC PD and a resistor can capture I_{ph} at 1 kHz during exposure, as shown in Fig 2B. Over a representative time period of 200s, the results in this case detected all pulses at a regular interval. SFig 3b shows I_{ph} sampled at 10 Hz and 1 Hz, where none of the pulses is captured at 1Hz.

The measurement response associated with the AMD module appears in Fig. 2C. A high bandwidth data acquisition system sampled V_{sc} at 1 kHz. Here, 20 UVC photodiodes
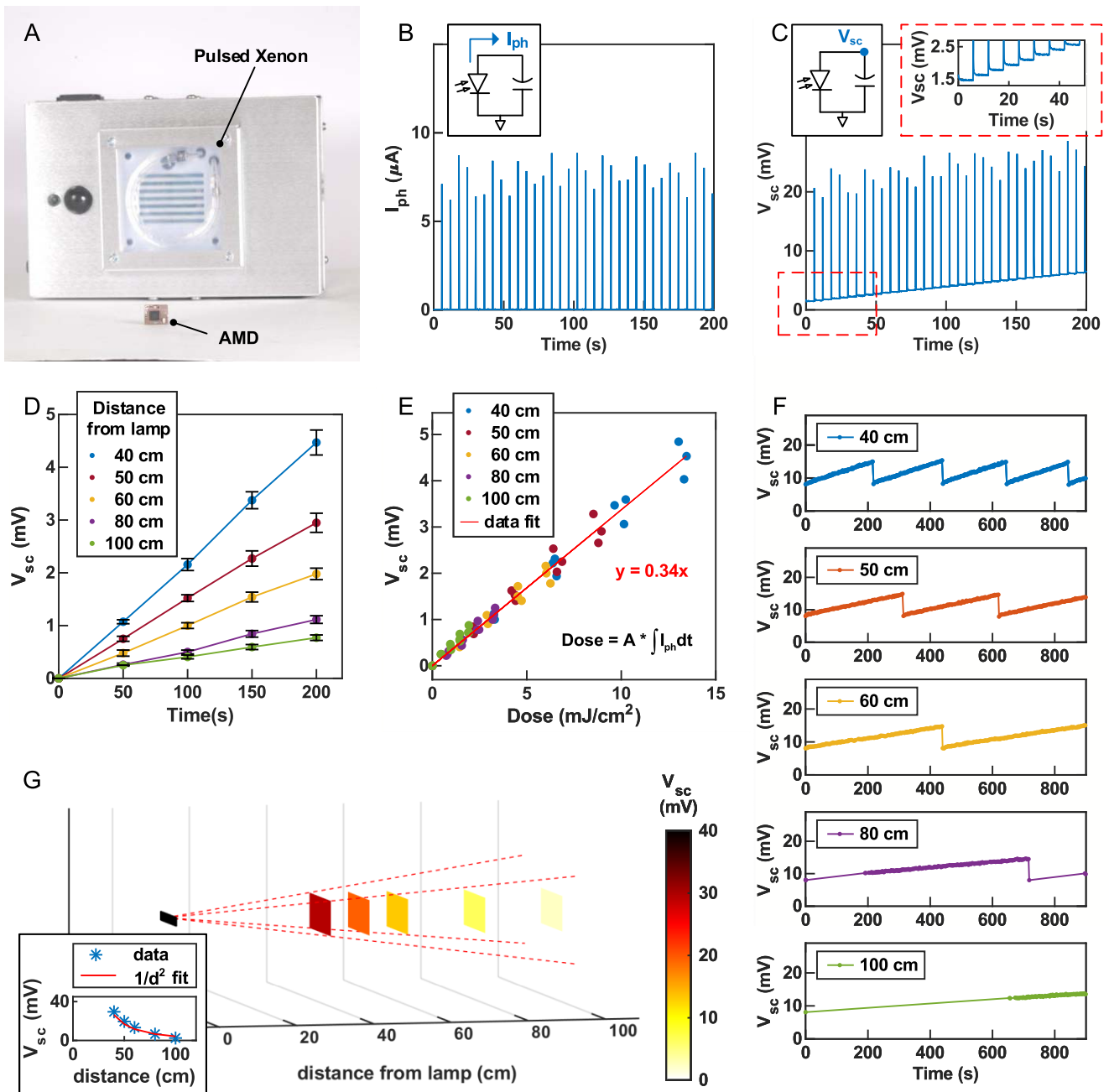
Fig. 2. **Detection of UVC dose from a pulsed Xenon Lamp.** (A) Photograph of an accumulation-mode dosimeter (AMD) and a pulsed Xenon lamp. (B) Photocurrent (I_{ph}) of a UVC photodiode as a function of time during exposure to a pulsed Xenon lamp. A high bandwidth data acquisition system sampled I_{ph} at 1kHz. Peaks correspond to Xenon pulses. (C) Supercapacitor voltage (V_{sc}) as a function of time during exposure to a pulsed Xenon lamp. A high bandwidth data acquisition system sampled V_{sc} at 1kHz. The inset highlights the stepwise increase of V_{sc} following the peaks. (D) V_{sc} as a function of time during exposure to the pulsed Xenon lamp at varied distances ($d = $ 40cm, 50cm, 60cm, 80cm, 100cm) sampled at 0.02Hz. Error bars represent standard deviation across 3 trials over 200s exposure periods. (E) Concatenated V_{sc} in (D) as a function of UVC dose. Dose $= A * \int I_{ph}dt$, where $A = 39$ [nA]/[mW/cm^2] and dt is the exposure time. The fitting result indicates a zero-intercept linear dependence of the concatenated data; the slope is 0.34 mV/(mJ/cm^2). (F) Wirelessly recorded supercapacitor voltage (V_{sc}) as a function of time during exposure to a pulsed Xenon lamp at varied distances ($d = $ 40cm, 50cm, 60cm, 80cm, 100cm). A smartphone (iPhone 7) received data via Bluetooth. (G) Spatial map of the cumulative sum of V_{sc} measured in (F). Inset plots the cumulative sum of V_{sc} as a function of d, and the fitting result indicates an inverse square law of light.

are in parallel to SCs with a total capacitance of 2.1mF. The base V_{sc} value increases in a stepwise manner, as expected, with sharp peaks (V_{peaks}) that are coincident with each pulse from the Xenon lamp. A circuit simulation of V_{sc} using experimentally observed values of I_{ph} from Fig 2B yields a similar response (SFig 4a-b). Additional measurements of I_{ph} and V_{sc}

at different distances ($d = $ 40 cm, 50 cm, 60 cm, 80 cm, and 100 cm) from the lamp are in SFig 5a-b. The device of Fig. 1 exploits this cumulative response to yield accurate measurements of dose, without any limitation associated with sampling rate. Accumulated V_{sc} (in SFig 4b) sampled at a 50 s interval as a function of exposure time for various d is in Fig 2D.

Error bars represent standard deviations across 3 trials over a 200s exposure period. Concatenated V_{sc} in Fig 2D as a function of UVC dose for various d is in Fig 2E. Linear conversion of I_{ph} (in SFig 4a) by a constant factor A defined by the PD (GUVC-S10GD; A = 39 [nA]/[mW/cm^2]) determines the UVC power. Numerical integration of UVC power over time yields UVC dose. Over a representative exposure time of 200 s, V_{sc} increases proportionally to UVC dose with a zero-intercept slope of 0.34 mV per 1 mJ/cm^2.

The cumulative sums of wirelessly measured values of V_{sc}, captured on a smartphone (iPhone 7) as a function of d for exposure times of 15 min, appear in Fig 2G. The results are consistent with the inverse square law ($\sim 1/d^2$) for an approximate point source, as shown in the inset of Fig 2G. The wireless data are in Fig 2F. During exposure to a pulsed Xenon lamp, V_{peaks} may trigger BLE SoC 'wake-up' events at each pulse if V_{peaks} exceeds V_{ref}. To read the accumulated V_{sc} following these peaks, the BLE SoC includes a reading delay (800 ms) in the measurement of V_{sc} following each 'wake-up' event. Discharge of the SC initiates only if the accumulated V_{sc} does not exceed V_{ref}. For battery optimization, V_{peaks} can be eliminated with a software bypass or with a hardware filter circuit, as simulated in SFig 4c-d. Additional wireless dosimetry results using four dosimeters to spatially map UVC dose from a pulsed Xenon lamp over a 30 min exposure period are in SFig 6. During these experiments, a single smartphone simultaneously collects data from multiple devices.

B. Multiwavelength Dosimetry of Various Germicidal Lamps

Multispectral dosimetry may be of interest because various types of UVGI lamps have different emission characteristics across the UV band. Traditional dosimeters for UVGI focus only on UVC. Since germicidal effects of irradiation are wavelength-specific, spectral assessments across UVA and UVB are additionally desirable for accurate assessment of germicidal power. UVGI applications typically rely on low pressure mercury vapor lamps or pulsed Xenon light sources [24], [25]. Emission from a Xenon arc device has broad spectral lines across the UVC, UCB and UVA, as well as the visible bands. The low-pressure mercury-arc lamp is a continuous light source that emits at 254 nm with full width at half maximum (FWHM) <15 nm. Light-emitting diodes (LEDs) with UVC specific radiation are another emerging alternative. Sources such as tungsten-halogen bulbs or UVB LEDs emit only trace percentages of UVC and are thus not ideal as an efficient germicide. In this study, a multichannel AMD (Fig 3A-B) with separate and simultaneous detection at UVA, UVB, and UVC wavelengths wirelessly measured exposure to various types of UVGI lamps. The Materials & Methods details the system architecture of a multi-channel AMD.

Wireless multi-wavelength measurements with a multi-channel AMD during exposure to a pulsed Xenon lamp and a low-pressure mercury-arc lamp are in Fig3 C-D. The ratio of the accumulated V_{sc} measured by UVA, UVB, and UVC channels (V_{sc_uvc}: V_{sc_uvb}: V_{sc_uva}) is 8 mV:6 mV:12 mV for pulsed Xenon and 8 mV:2 mV:0 mV for low-pressure mercury-arc lamp. The Xenon lamp generates a response across all three channels, consistent with its broadband UV operation. The low-pressure mercury-arc produces dominant responses in the UVC channel but not in the UVA. Due to overlapping detection spectra associated with the UVC and UVB PDs, the AMD also responds to some extent to UVB exposure. Connecting the output of the UVA detection channel to the LPCOMP establishes a UVA-triggered device, with responses during exposure to UV LEDs in SFig 7a-b.

Measurements with a multi-wavelength dosimeter during exposure with a Xenon lamp highlights wavelength dependent effects that result from passing the light through borosilicate glass (BO150, thickness 150 μm; BO300, thickness 300 μm) in Fig 3E. The ratio of accumulated V_{sc} without and with these filters corresponds to a percentage transmission (%T). Multichannel AMD measurements of %T weighted by spectral responsivity of UV PDs are in Fig 3F. For UVC, UVB and UVA, the values for BO150 (%T_{BO150}) at wavelengths of peak responsivity are 65%, 82%, and 96%, respectively, and the values for BO300 (%T_{BO300}) are 44%, 67%, and 90%, respectively. The observed trend approximately follows %T_{BO300} = (%T_{BO150})^2. Transmission properties measured using a UV spectrometer (Lambda 1050, PerkinElmer) for both filters are also in Fig 3F. The wirelessly received data are in SFig 7c-e.

C. UVC Dosimetry During E. Coli Disinfection

Accurate measurements of UVC dose are important in assessments of germicidal efficacy. Demonstrations in this context rely on exposure of discs concentrated with *Escherichia coli* (E. Coli) to low-pressure mercury-arc, with simultaneous measurements of dose, as in the schematic diagram in Fig 4A. The dosimeter here supports 50 UVC photodiodes in parallel to SCs with a total capacitance of 2.1 mF. A commercial IMD measured intensity before and after the process to provide comparative data. Experiments include discs (n = 3) exposed for six different durations (t = 30s, 1min, 3min, 5min, 10min, 15min), labelled trial A through F in an order of increasing exposure time.

Exposure doses measured by the AMD and those inferred from the IMD for each trial are in Fig 4C. Wirelessly received AMD data with light-adaptive sampling is in SFig 8. A trapezoidal integration of intensities measured by the IMD over exposure time yields the dose. A linear calibration factor of 0.22 [mJ/cm^2]/mV converts the total accumulated V_{sc} measured by the AMD to exposure dose per unit area. A calibration plot is in SFig9. The dose measured by AMD for trials A-F are 3.7 mJ/cm^2, 6.9 mJ/cm^2, 24.0 mJ/cm^2, 40.3 mJ/cm^2, 78.0 mJ/cm^2, and 116.8 mJ/cm^2. The corresponding IMD doses are 4.4 mJ/cm^2, 9.2 mJ/cm^2, 27.3 mJ/cm^2, 45.3 mJ/cm^2, 92.1 mJ/cm^2, and 133.7 mJ/cm^2.

Effective UVGI relies on delivery of a target dose. Presence or absence of active bacteria on treated *E* Coli discs indicates germicidal effectiveness for trials A through F. The experiments involve irradiated discs suspended in culture medium for 22 hours while shaken to incubate bacteria. A diagram of experimental procedure described in Materials & Methods is in Fig 4B. A blank disc without E. Coli and
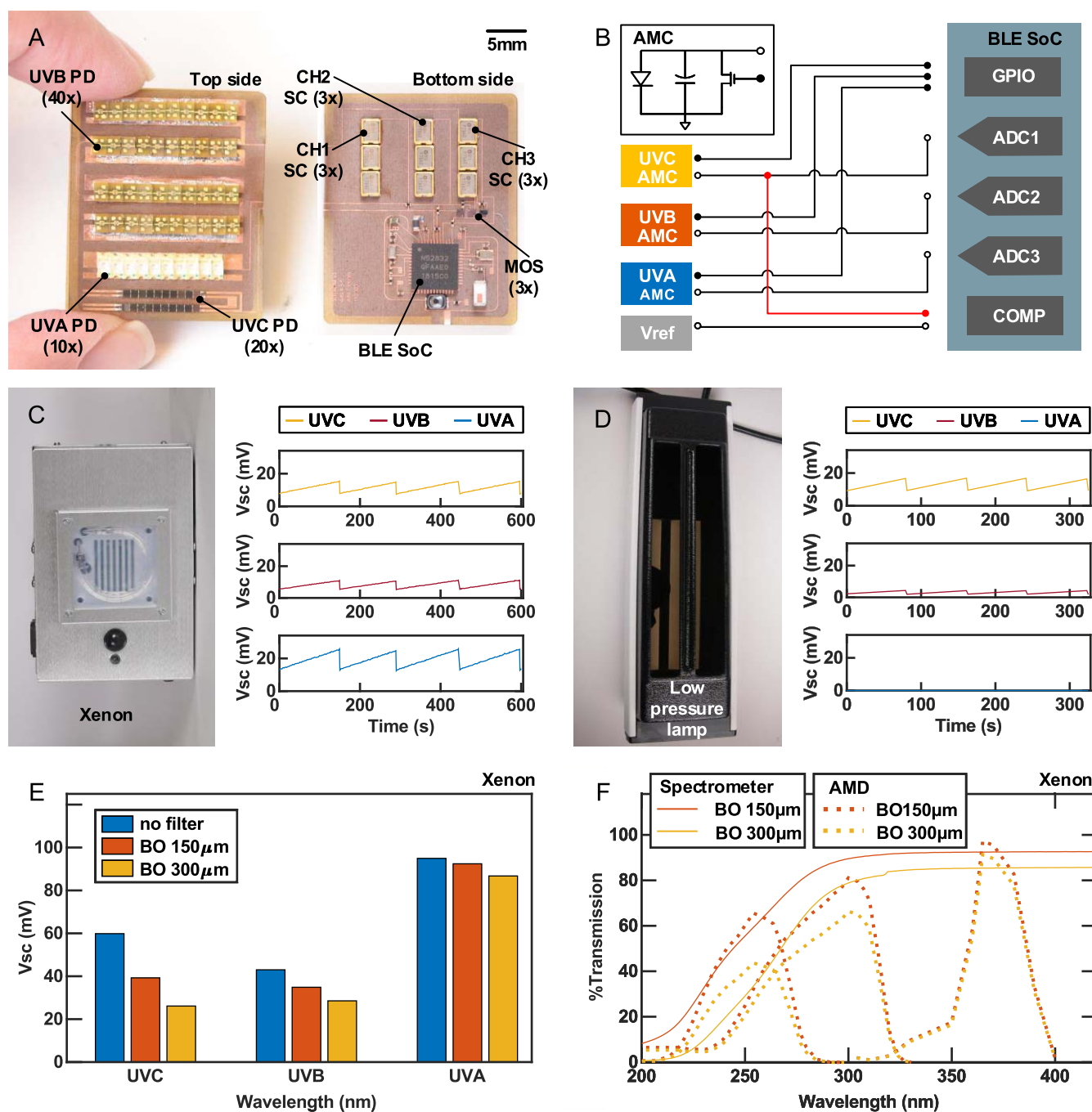
Fig. 3. **Detection of UVA, UVB, and UVC doses with a multichannel, wireless dosimeter.** (A) Photograph of a 3-ch, accumulation-mode dosimeter (AMD). Top and bottom sides are shown. The top side contains photodiode arrays of UVA, UVB, and UVC. The bottom side supports a Bluetooth system-on-chip (BLE SoC), supercapacitors (SC), MOSFETs (MOS), and auxiliary components. (B) Block diagram of a 3-channel AMD with UVA, UVB, and UVC detection channels connected to the BLE SoC. Each accumulation-mode channel (AMC) consists of PDs, SCs, and a MOS. V_{sc} of UVC AMC, UVB AMC, and UVA AMC connects to three separate ADCs of BLE SoC. A single GPIO of the BLE SoC controls the MOSFETs of all three AMCs. UVC AMC connected to LPCOMP of the BLE SoC established UVC as the trigger channel to 'wake' BLE SoC if V_{sc} of UVC AMC exceeds V_{ref}, where V_{ref} is a preset threshold voltage. The BLE SoC remains in 'deep-sleep' if V_{sc} of UVC AMC $< V_{ref}$. For V_{sc} of UVC AMC $> V_{ref}$, the BLE SoC 'wakes up', reads all three ADCs, wirelessly transmits all three V_{sc} values, discharges the SCs via GPIO activation, and returns to 'deep-sleep' if V_{sc} of UVC AMC $< V_{ref}$. (C,D) Wireless measurements during exposure to a pulsed Xenon lamp and to a low-pressure mercury-arc lamp. A smartphone (iPhone 7) received data via Bluetooth. (E) Accumulated V_{sc} wirelessly measured by the 3-ch AMD during exposure to a pulsed Xenon lamp without and with borosilicate (BO) filters of thicknesses 150μm and 300μm. (F) %Transmission of BO filters of thicknesses 150μm and 300μm as a function of wavelength measured by a 3-ch AMD and measured by a spectrometer. The 3-ch AMD measurement is a ratio of accumulated V_{sc} with a filter to without a filter in (E) weighted by responsive spectrum of corresponding PDs.

an un-irradiated disc with E. Coli serve as negative and positive controls, respectively. Photographs of E. Coli discs cultured overnight after UVC exposure are in Fig 4D. After

incubation, an OD600 measurement quantifies the bacteria density. OD600 measurements for these cultures are in Fig 4E. Indicated error bars represent standard deviation across three
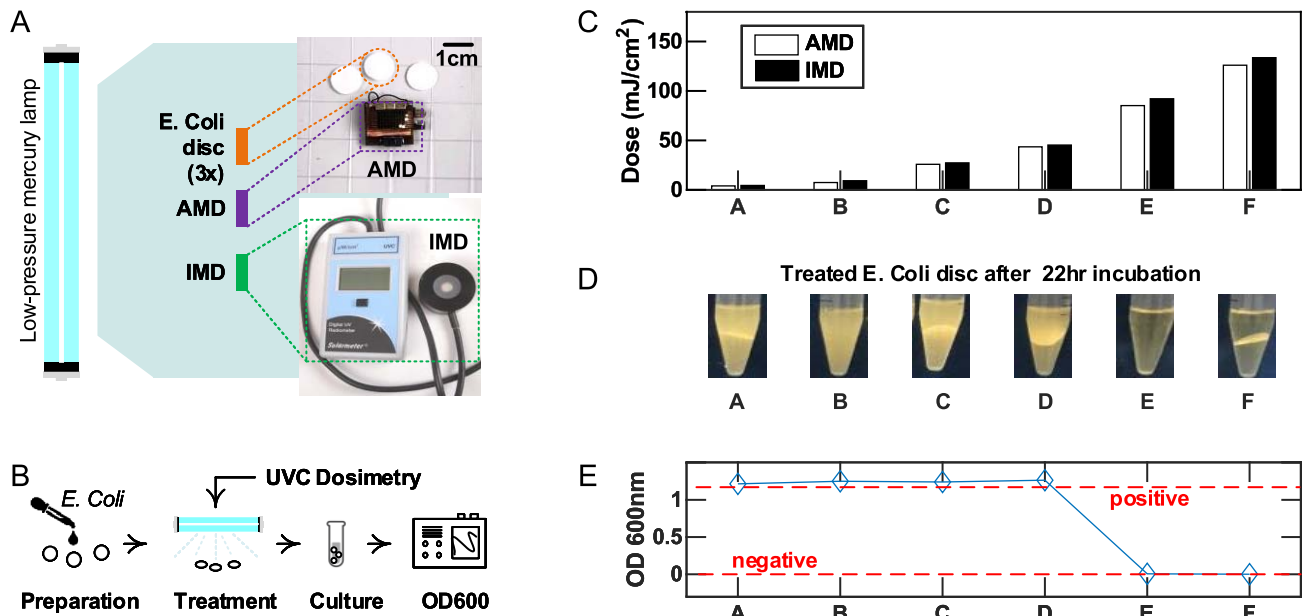
Fig. 4. UVC dosimetry during disinfection of E. Coli (A) Schematic illustration of the experimental setup. A low pressure mercury-arc lamp exposed an intermittent-mode detector (IMD; UVC 8.0, Solarmeter), an accumulation-mode dosimeter (AMD), and E. Coli disks (n = 3; diameter = 10mm) for varied times (t = 30s, 1min, 3min, 5min, 10min, and 15min) corresponding to trials labelled A through F. A button-operated IMD measured UVC power before and after each trial. An AMD wirelessly measured exposure dose during each trial. The orthogonal distance between the lamp and E. Coli disks is 35cm. (B) Schematic illustration of the experimental procedure. (C) UVC doses for trials A through F measured using AMD and IMD. IMD dose is extrapolated as a trapezoidal integration of measured UVC power over corresponding exposure times. AMD dose is extrapolated as B* cumulative sum of V_{sc}, where B is 0.22 [mJ/cm^2]/mV. (D) Photographs of irradiated E Coli disks in culture medium after 22hour incubation. (E) OD600 of samples in (D). OD600 of positive and negative controls are indicated in red. Positive control was unirradiated E. Coli disk and negative control was blank disk. Error bars represent standard deviation over three samples.

simultaneously exposed discs. The OD600 of positive and negative controls are 1.2 and 0.001, respectively. Trials with measured UVC doses of 88.0mJ/cm^2 and greater yield OD600 < 0.1, suggesting successful disinfection. Samples A through D with measured UVC doses of 45.3 mJ/cm^2 and less returns OD600 >1, indicating ineffective disinfection.

IV. TECHNOLOGY LIMITATIONS

The response times of the PDs used in these systems define the limits for pulse detection. The detection limit of Aluminum Gallium Nitride (AlGaN) PDs used here for UVC detection is in the nanosecond regime [26]. Main sources of error are in electrical leakage associated with the SCs. Defining a small threshold voltage for discharging the SCs can minimize this effect. In this study, the selected threshold voltage (V_{ref}) is 17mV. The current platform incorporates an on-board memory module to store and transmit accumulated voltage values from up to three previous 'wake-up' events, thereby mitigating loss of data when wireless connectivity is poor.

V. CONCLUSION

The technology introduced here supports continuous monitoring of exposure dose associated with germicidal lamps at single and at multiple wavelengths, including those that generate short pulses of light in the UVC spectrum. Results are experimental demonstrations of sensor platforms that enable 1) accurate UVC dosimetry of a pulsed Xenon lamp with millisecond pulses sampled at long intervals (>1s), and 2) simultaneous multispectral dosimetry of various UVGI

sources across UVA, UVB, and UVC regimes. Alignment of fabrication processes and components for these devices with standards in semiconductor manufacturing suggests strong potential for scaled, cost effective deployment.

In traditional systems, the trade-off between measurement accuracy and sampling rate constrains the operational lifespan of battery-powered devices for dosimetry and related sensing applications. IMD at a high sampling frequency places demands on memory storage capacity and data processing. For example, a commercial electronic dosimeter (UVA dosimeter, Scienterra) sampling every 2s offers a memory capacity of 6 days and a battery life of 1.2 months with a 3V coin cell battery (CR3216), assuming continuous exposure 12 h per day. The same dosimeter sampling every 1 min has memory capacity and battery life for operation over 6 months and 1.1 year, respectively. [27] Alternatively, AMDs can accurately detect UVGI irrespective of sampling interval. As result, an AMD implemented with a light-adaptive sampling scheme, as opposed to use of time-based sampling at high frequency, increases the sampling interval and reduces the data volume, to extend deployment lifetime while enabling continuous UVGI sensing.

Pulsed germicidal lamps are powerful tools for reducing microbial and viral load on surfaces in hospital settings. Capabilities for practical dosimetry from germicidal lamps are important for reliable and effective disinfection. In addition to monitoring UVGI in healthcare, other applications include monitoring during UV sterilization of food or water, UV disinfection of public spaces such as subways or bathrooms, or at-home disinfection of surfaces.

ACKNOWLEDGMENT

Seung Yun Heo is with the Department of Biomedical Engineering, Northwestern University, Evanston, IL 60208 USA (e-mail: simoneheo@gmail.com).

Kyeongha Kwon is with the Department of Electrical Engineering, Korea Advanced Institute of Science and Technology, Daejeon 34141, Republic of Korea (e-mail: kyeongha@kaist.ac.kr).

Michelle Chan was with the Department of Biomedical Engineering, Northwestern University, Evanston, IL 60208 USA. She is now with the Querrey Simpson Institute for Bioelectronics, Evanston, IL 60208 USA (e-mail: michellechan2020@u.northwestern.edu).

Philipp Gutruf and Alex Burton are with the Department of Biomedical Engineering, The University of Arizona, Tucson, AZ 85721 USA (e-mail: pgutruf@arizona.edu; alexburton@arizona.edu).

Tony Banks is with the Querrey Simpson Institute for Bioelectronics, Evanston, IL 60611 USA (e-mail: tbanks@northwestern.edu).

Chongwen Duan is with the Department of Biomedical Engineering, Northwestern University, Evanston, IL 60208 USA (e-mail: c-duan@northwestern.edu).

Hokyung Jang is with the Department of Electrical and Computer Engineering, University of Wisconsin–Madison, Madison, WI 53706 USA (e-mail: janghk51@gmail.com).

Jeonghyun Kim is with the Department of Electronics Convergence Engineering, Kwangwoon University, Seoul 01897, Republic of Korea (e-mail: jeonghyun09@gmail.com).

Daniel Franklin was with the Querrey Simpson Institute for Bioelectronics, Evanston, IL 60208 USA. He is now with the Institute of Biomedical Engineering, University of Toronto, Toronto, ON M5S 3G9, Canada (e-mail: dan.franklin@northwestern.edu).

Jun Bin Park is with Sibel Inc., Evanston, IL 60201 USA (e-mail: junbin.park@gmail.com).

John A. Rogers is with the Department of Materials Science and Engineering, the Department of Biomedical Engineering, and the Department of Neurological Surgery, Northwestern University, Evanston, IL 60208 USA (e-mail: jrogers@northwestern.edu).

REFERENCES

[1] *Implementing Filtering Facepiece Respirator (FFR) Reuse, Including Reuse after Decontamination, When There Are Known Shortages of N95 Respirators*, Centers for Disease Control and Prevention, Atlanta, GA, USA, 2020.

[2] J. J. Whalen, "Environmental control for tuberculosis; basic upper-room ultraviolet germicidal irradiation guidelines for healthcare settings guide," Centers Disease Control Prevention, Atlanta, GA, USA, Tech. Rep. 2009-105, 2009.

[3] I. H. Hamzavi *et al.*, "Ultraviolet germicidal irradiation: Possible method for respirator disinfection to facilitate reuse during the COVID-19 pandemic," *J. Amer. Acad. Dermatol.*, vol. 82, no. 6, pp. 1511–1512, Jun. 2020.

[4] H. Yang, J. Hu, P. Li, and C. Zhang, "Ultraviolet germicidal irradiation for filtering facepiece respirators disinfection to facilitate reuse during COVID-19 pandemic: A review," *Photodiagnosis Photodynamic Therapy*, vol. 31, Sep. 2020, Art. no. 101943.

[5] A. Besaratinia, J. Yoon, C. Schroeder, S. E. Bradforth, M. Cockburn, and G. P. Pfeifer, "Wavelength dependence of ultraviolet radiation-induced DNA damage as determined by laser irradiation suggests that cyclobutane pyrimidine dimers are the principal DNA lesions produced by terrestrial sunlight," *FASEB J.*, vol. 25, no. 9, pp. 3079–3091, Sep. 2011.

[6] N. G. Reed, "The history of ultraviolet germicidal irradiation for air disinfection," *Public Health Rep.*, vol. 125, no. 1, pp. 15–27, Jan. 2010.

[7] D. Voet, W. B. Gratzer, R. A. Cox, and P. Doty, "Absorption spectra of nucleotides, polynucleotides, and nucleic acids in the far ultraviolet," *Biopolymers*, vol. 1, no. 3, pp. 193–208, Jun. 1963.

[8] S. B. Martin, Jr., C. Dunn, J. D. Freihaut, W. P. Bahnfleth, J. Lau, and A. Nedeljkovic-Davidovic, "Ultraviolet germicidal irradiation: Current best practices," *Ashrae J.*, vol. 50, no. 8, p. 28, 2008.

[9] S. E. Beck, R. A. Rodriguez, M. A. Hawkins, T. M. Hargy, T. C. Larason, and K. G. Linden, "Comparison of UV-induced inactivation and RNA damage in MS2 phage across the germicidal UV spectrum," *Appl. Environ. Microbiol.*, vol. 82, no. 5, pp. 1468–1474, Mar. 2016.

[10] H. Woo *et al.*, "Efficacy of inactivation of human enteroviruses by dual-wavelength germicidal ultraviolet (UV-C) light emitting diodes (LEDs)," *Water*, vol. 11, no. 6, p. 1131, May 2019.

[11] S. E. Beck, N. M. Hull, C. Poepping, and K. G. Linden, "Wavelength-dependent damage to adenoviral proteins across the germicidal UV spectrum," *Environ. Sci. Technol.*, vol. 52, no. 1, pp. 223–229, Jan. 2018.

[12] I. Kohli *et al.*, "UVC germicidal units: Determination of dose received and parameters to be considered for N95 respirator decontamination and reuse," *Photochem. Photobiol.*, vol. 96, no. 5, pp. 1083–1087, Sep. 2020.

[13] D. Irving, D. A. Lamprou, M. Maclean, S. J. MacGregor, J. G. Anderson, and M. H. Grant, "A comparison study of the degradative effects and safety implications of UVC and 405 nm germicidal light sources for endoscope storage," *Polym. Degradation Stability*, vol. 133, pp. 249–254, 2016.

[14] W. G. Lindsley *et al.*, "Effects of ultraviolet germicidal irradiation (UVGI) on N95 respirator filtration performance and structural integrity," *J. Occupational Environ. Hygiene*, vol. 12, no. 8, pp. 509–517, Aug. 2015.

[15] D. Ozog *et al.*, "The importance of fit testing in decontamination of N95 respirators: A cautionary note," *J. Amer. Acad. Dermatol.*, vol. 83, no. 2, pp. 672–674, Aug. 2020.

[16] H. Junker, P. Lukowicz, and G. Troster, "Sampling frequency, signal resolution and the accuracy of wearable context recognition systems," in *Proc. 8th Int. Symp. Wearable Comput.*, vol. 1, Oct. 2004, pp. 176–177.

[17] M. M. Nerandzic *et al.*, "Evaluation of a pulsed xenon ultraviolet disinfection system for reduction of healthcare-associated pathogens in hospital rooms," *Infection Control Hospital Epidemiol.*, vol. 36, no. 2, pp. 192–197, Feb. 2015.

[18] M. Stibich *et al.*, "Evaluation of a pulsed-xenon ultraviolet room disinfection device for impact on hospital operations and microbial reduction," *Infection Control Hospital Epidemiol.*, vol. 32, no. 3, p. 286, 2011.

[19] W. Luo, A. Chen, M. Chen, W. Dong, and X. Hou, "Comparison of sterilization efficiency of pulsed and continuous UV light using tunable frequency UV system," *Innov. Food Sci. Emerg. Technol.*, vol. 26, pp. 220–225, Dec. 2014.

[20] H. Ogihara, K. Morimura, H. Uruga, T. Miyamae, M. Kogure, and S. Furukawa, "Inactivation of food-related microorganisms in liquid environment by pulsed xenon flash light treatment system," *Food Control*, vol. 33, no. 1, pp. 15–19, Sep. 2013.

[21] S. Y. Heo *et al.*, "Wireless, battery-free, flexible, miniaturized dosimeters monitor exposure to solar radiation and to light for phototherapy," *Sci. Transl. Med.*, vol. 10, no. 470, Dec. 2018, Art. no. eaau1643.

[22] K. Kwon *et al.*, "Miniaturized, light-adaptive, wireless dosimeters autonomously monitor exposure to electromagnetic radiation," *Sci. Adv.*, vol. 5, no. 12, Dec. 2019, Art. no. eaay2462.

[23] A. Krause *et al.*, "Trading off prediction accuracy and power consumption for context-aware wearable computing," in *Proc. 9th IEEE Int. Symp. Wearable Comput. (ISWC)*, Oct. 2005, pp. 20–26.

[24] S. Wengraitis *et al.*, "Pulsed UV-C disinfection of Escherichia coli With light-emitting diodes, emitted at various repetition rates and duty cycles," *Photochem. Photobiol.*, vol. 89, no. 1, pp. 127–131, Jan. 2013.

[25] S. L. Miller, J. Linnes, and J. Luongo, "Ultraviolet germicidal irradiation: Future directions for air disinfection and building applications," *Photochem. Photobiol.*, vol. 89, no. 4, pp. 777–781, Jul. 2013.

[26] G. Xu *et al.*, "High speed, low noise ultraviolet photodetectors based on GaN pin and AlGaN (p)-GaN (i)-GaN (n) structures," *Appl. Phys. Lett.*, vol. 71, no. 15, pp. 2154–2156, 1997.

[27] M. W. Allen, N. Swift, K. M. Nield, B. Liley, and R. L. McKenzie, "Use of electronic UV dosimeters in measuring personal UV exposures and public health education," *Atmosphere*, vol. 11, no. 7, p. 744, Jul. 2020.